# Spatial Spectroscopy for Hall Thruster Plasma Characterization

#### IEPC-2025-630

Presented at the 39th International Electric Propulsion Conference Imperial College London • London, United Kingdom 14-19 September 2025

Ian J. Hofbeck<sup>1</sup> and Richard E. Wirz<sup>2</sup>

Plasma, Energy, & Space Propulsion Lab; Oregon State University, Corvallis, Oregon, 97331, USA

Spatial spectroscopy was performed on a Hall Effect Thruster plume using a monochrome low-light camera equipped with narrow bandpass filters to investigate the distribution of ion and neutral species in the plume of a thruster with a center mounted cathode. Standard Optical Emission Spectroscopy (OES) was used to scale relative intensities of each image with respect to the overall spectra. In this work we examine the filtered images qualitatively, and quantitatively with processing techniques including inverse Abel transforms to compute radial intensity profiles of the plasma. Images taken with different wavelength filters for ions and neutrals were aligned and compared to show intensity ratios between ions and neutrals, alluding to regions of increased ionization. Noticeable differences in photon emission characteristics are found between excited neutral and excited ion species, both near the exit plane of the thruster and further downstream. These results demonstrate that SpatialOES can provide valuable insight to plasma and plume characterization of the interplay between ions, neutrals, and electrons for Hall thrusters and other EP devices.

## I. Introduction

Characterizing the distribution of plasma species and plume dynamics of Hall Effect Thrusters (HETs) are important areas of research in electric propulsion requiring advanced non-intrusive diagnostics with high spatial resolution and diagnostics that are device-agnostic. HET performance is affected by many factors including cathode placement, operating conditions, and facility conditions. Several efforts aim to understand and model the effects of a facility on thruster operation, such as including background neutral density<sup>1</sup>. SpatialOES provides a wide-field non-intrusive diagnostic method to record plasma plumes and how they are affected by neutral density. Spatial spectroscopic capabilities can also be applied to other EP devices like gridded ion thrusters (GITs) to collect information on near-field plume beam density. This would provide data for a reduced order predictive engineering model (PEM) being developed within our research group, the Plasma, Energy, and Space Propulsion Laboratory (PESPL) at Oregon State University<sup>2</sup>. Applying SpatialOES to different propellants, including xenon and krypton, can be used to compare results with high order plume models, such as the Hall2De model, developed by Jet Propulsion Laboratory and the University of Michigan<sup>3</sup>.

The performance of a HET is influenced by the coupling relationship between its anode discharge channels and the cathode<sup>4-6</sup>. The placement of the cathode plays a major role in its coupling to the anode, and in turn affects thruster performance<sup>7-10</sup>. Cathodes are typically either placed external to the thruster, or internally through the center of the thruster to be flush with the exit plane. Researchers have investigated the effects of internal versus external cathode placement, and internal cathodes typically lead to more efficient thruster performance. However, the benefits are often

<sup>&</sup>lt;sup>2</sup> Professor, Mechanical Engineering, Richard.wirz@oregonstate.edu



The 39<sup>th</sup> International Electric Propulsion Conference, Imperial College London, London, United Kingdom 14-19 September 2025

<sup>&</sup>lt;sup>1</sup> Graduate Student, Mechanical Engineering, hofbecki@oregonstate.edu

dependent on the size or operating conditions of the thruster. For external cathodes placed very close to the anode, orientation has a strong effect on efficiency, due to the influence of the strong magnetic fields from the nearby thruster<sup>7</sup>. Cathode thruster coupling is also affected by facility pressure<sup>11-13</sup>.

Spatial spectroscopy can be paired with plasma models and collisional radiative models (CRMs) to gain important insight into HET plasma behavior. These models estimate electron density and electron temperature using excitation rate coefficients, which are dependent on OES information<sup>14,15</sup>. Using data obtained from spatial spectroscopy with CRMs can allow for a spatially resolved distribution of electron temperature and density, which would be especially valuable for another research effort in the PESPL group focusing on xenon collisional radiative mechanisms in radio frequency (RF) thrusters<sup>16,17</sup>. We also plan to use these efforts to inform and leverage Kr CRM efforts led by Vernon Chaplin<sup>14</sup> at NASA JPL and Azer Yalin at Colorado State University.

"SpatialOES" is a technique by which filtered images using narrow filters enable observations of desired wavelengths to provide *spatially resolved* optical emission spectroscopy (OES) data. This method was used previously by Konopliv, Johnson, and Wirz to observe the SPT-70 HET using different gas combinations, Xe and Kr, for the anode and external cathode <sup>18</sup>. Similar filtered-imaging studies on external cathodes have been conducted by Zhang, et al. <sup>19</sup>. While both studies visualized the interactions between the anode and cathode for thrusters with an externally mounted cathode, the present work focuses on a 9 kW HET with an internally mounted cathode. For SpatialOES we are observing excited species, which are excited by electrons, thus the spectral intensity correlates to electron excitation and species density.

The objective of this study is to find the distribution of excited ions and neutrals in a HET with a center-mounted cathode using SpatialOES and image analysis. The approach taken was first to record spatial distributions of plasma species in a HET test, then compare the images both qualitatively and with image processing techniques at key locations in the plume. Traditional OES was also used to measure the light across the plume center, in order to compare the scale of light intensity with the filtered images.

# II. Approach and Key Processes

High resolution images were first taken with narrow band-pass filters for specific wavelengths associated with plasma species of interest, in this case krypton neutrals and singly charged ions for coupled cathode-HET plumes. To get a relative scale of brightness to match across all images, steady OES measurements at specific points in the plume were recorded to scale each photograph's brightness relative to the intensity counts recorded by the spectrometer. To analyze the filtered images quantitatively, the next step of the approach was to divide the plume image into vertical slices, and compare brightness as a function of image height across the plume. This study also used an inverse Abel transform on those vertical slices to estimate the radial distribution of species emission at different lengths along the plume. The images were also compared qualitatively to assess similarities and differences in spatial species distributions from this internal cathode test with previous external cathode studies.

#### A. Background: OES and Krypton

Excited ions and neutrals are subject to spontaneous radiative decay, where an electron will transition from excited levels down to lower energy levels, conserving energy in the form of an emitted photon. The wavelength of this photon is directly related to the drop in energy made by the electron from one quantized energy state to another. Both krypton ions and krypton neutral atoms have their own set of quantized electron energy levels and wavelengths emitted during a plasma discharge. This means that we can distinguish between neutral krypton, (KrI), and singly ionized krypton (KrII) based on the wavelengths of light emitted in the plasma. Figure 1 shows an energy level diagram for neutral Kr atoms<sup>20</sup>, and an example of spectral data collected on krypton plasma during this study. The 811.3 nm and 829.8 nm transitions are illustrated on both diagrams<sup>21</sup>. Optical Emission Spectroscopy (OES) is used to measure the relative intensity of each wavelength.



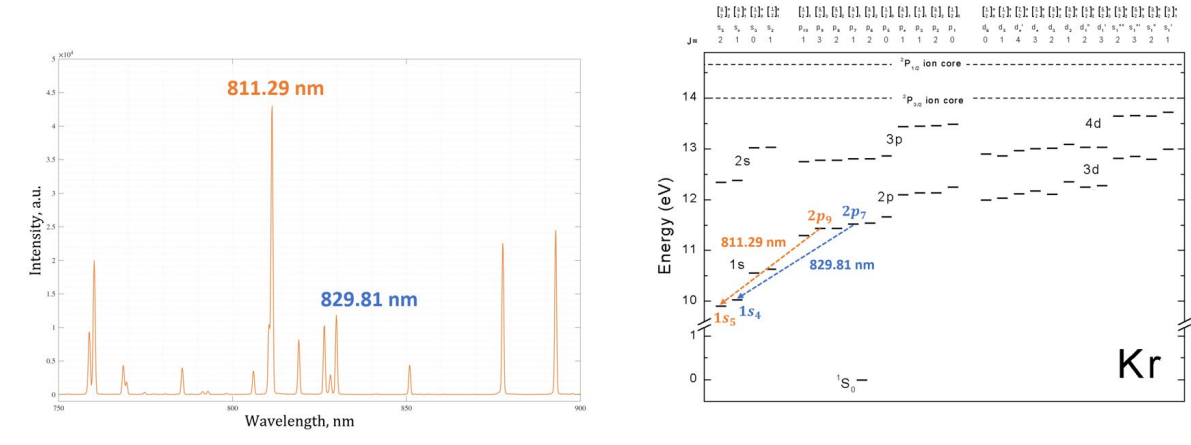


Figure 1. (left) OES data collected during the Kr thruster test. (right) Energy level diagram<sup>20</sup> for neutral Kr with illustration for 811.3 nm and 829.8nm transitions.

## B. Background: Wavelengths of Choice

several wavelengths were selected to represent both neutrals and ions. For krypton, the most prominent neutral lines lie in the 800 to 900 nm near-infrared (NIR) region, while the most prominent ion lines lie in the 400 to 500 nm visible light region. Wavelengths of interest were determined from previous RF plasma tests for projects motivated by the Air Force Office of Scientific Research (AFOSR)<sup>22</sup>. The wavelengths used for this study are shown below in Fig. 2, and were chosen based on relative intensity, and isolation from nearby emission lines. A wavelength of high relative intensity will provide a high signal to noise ratio in the output images. Isolated wavelengths ensure the camera's filter will only be passing one wavelength through to the image sensor, without any other peaks present. The top row of graphs is from spectral data available from the National Institute of Standards and Technology (NIST) to show both the target wavelength and those nearby<sup>23</sup>. The bottom two graphs show OES data recorded during the experiment, illustrating the relative intensity of all wavelengths together. Note the five times scale difference in Y axis between the neutrals on the right and ions on the left. One observation to be made about the 811.29 nm plot in Fig. 2 is that the NIST database shows a significantly higher peak at 810.44 nm, but in the real OES data taken during the test, that peak was overshadowed by about 4 times by the peak at 811.29 nm.

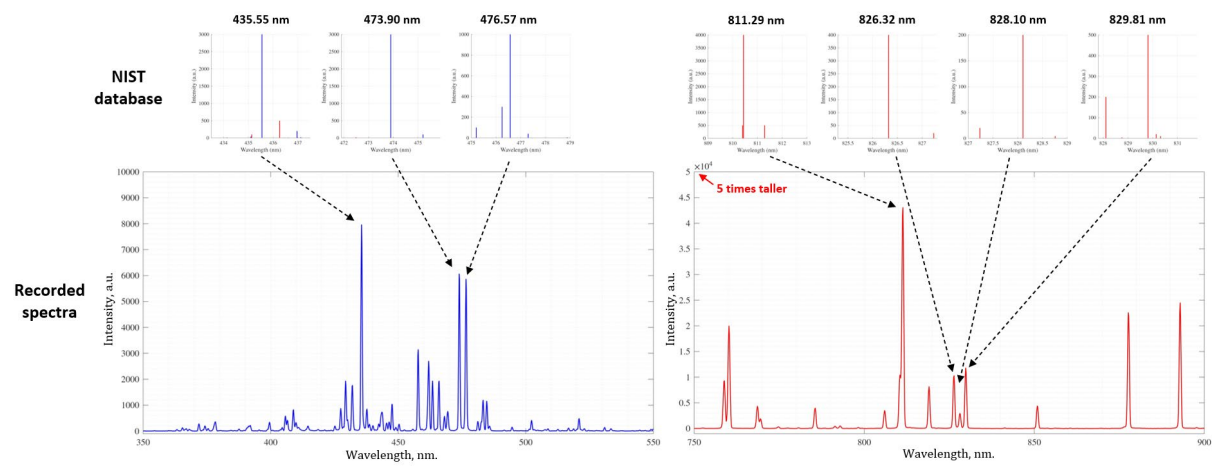


Figure 2. Comparing wavelengths of krypton ions in blue (left), and neutrals in red (right), between database spectra from NIST<sup>23</sup> and experimentally measured data.



#### C. Background: Inverse Abel Transform

A profile of brightness as a function of height can be obtained by taking a single vertical slice of pixel data from the filtered plasma images. Using the vertical profile, we can use tomographic reconstruction methods to retrieve a cross section profile of brightness density as a function of radius. The method used in this study is an inverse Abel transform, which is often employed for optical measurements of plasma plumes since it assumes radial symmetry.

An inverse Abel transform depends on a profile of signal through a density with respect to height. For plasma experiments, this is often achieved by recording OES data from a probe on a moving stage that can sweep across the plume height to get many parallel measurements<sup>24-26</sup>. For this experiment, we used one column of the filtered images to represent many parallel OES measurements. This method requires the lines of sight to the camera be as parallel as possible, so a high focal length telephoto lens is preferred. One column of image data can be considered to be signal as a function of height z, or F(z). In order to find the original radial density function f(r), The inverse Abel transform is given by Eq. (1).

$$f(r) = -\frac{1}{\pi} \int_{r}^{\infty} \frac{dF(z)}{dz} \frac{1}{\sqrt{z^2 - r^2}} dz \tag{1}$$

The inverse Abel transform is a simplification of the inverse Radon transform, which is naturally ill-posed and very vulnerable to noise<sup>27</sup>. The transform was performed in MATLAB as an inverse radon transform on the F(z) image data. To combat noise, the raw image data was smoothed in MATLAB using a Gaussian-weighted moving average filter.

# III. Test and Experimental Setup

The H9 HET test that we participated in was part of the FIT-III (Facility Interpolation Test) campaign. FIT-III was a collaborative research effort between University of Michigan, Georgia Tech, Colorado State University, and Oregon State University. For this test, the H9 was ignited at the Aerospace Corporation's EP3 test facility, which is roughly 4.25 meters in diameter and 9 meters long and equipped with a custom cryopump system capable of reaching base pressures of about  $1 \times 10^{-8}$  Torr with an effective pumping speed of 1ML/s on xenon.

Figure 3 shows a top-view diagram of the testing setup. The camera was placed in front of the viewing port in line with the thruster exit plane. The 13 cm diameter quartz viewing point was about 221 cm away from the thruster. From the opposite side of the camera, a collimating lens looked through the center of the thruster and cathode in order to record OES spectra. The camera used for this experiment was a low-light camera with a telephoto lens and an in-line filter holder. Two spectrometers were used to measure the ions and neutrals respectively. The first spectrometer, focused on the ions, had a wavelength range of 250 to 750 nm, and a 0.7 nm resolution. The second spectrometer, focused on the neutrals, had a wavelength range of 600 to 1100 nm and a 0.6 nm resolution. The collimating lens was lower than the thruster, facing up 45 degrees to cross the plume center. A laser was used to align the lens to the center of the thruster, and the diagram on the right in Fig. 3 shows the orientation of the probe with respect to the thruster.

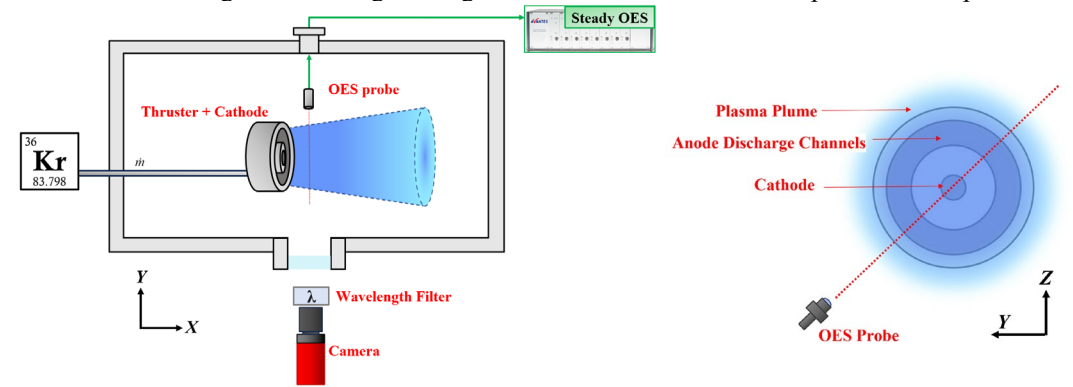


Figure 3. (left) Overall setup of filtered imaging test to show camera and OES arrangement, not to scale. (right) OES collimating lens arrangement looking across the thruster plume, not to scale.



#### IV.Results and Discussion

A set of seven filtered images were taken during the first test condition of the H9 thruster. Table 1 shows the test conditions at the time, and Fig. 4 shows the side view of the thruster plume, taken from a color DSLR camera. We note that the facility pressure conditions were high for H9 operation, with a measured background pressure of  $4 \times 10^{-5}$  Torr. For a reference of scale, the H9 thruster is known to run at background pressures between 2 - 10  $\mu$ Torr with xenon<sup>28</sup>. These measurements were taken at a preliminary operating condition prior to a larger test campaign aimed at exploring varying background pressures.

| Table 1. | Test | conditions | of the | H9 | thruster |
|----------|------|------------|--------|----|----------|
|          |      |            |        |    |          |

| Facility Pressure | P     | $V_D$ | $I_D$ | ṁ <sub>cat</sub> | $\dot{\mathrm{m}}_{an}$ |
|-------------------|-------|-------|-------|------------------|-------------------------|
| [Torr]            | [W]   | [V]   | [A]   | [sccm Kr]        | [sccm Kr]               |
| 4.0E-5            | 4,500 | 300   | 15    | 12.25            | 175                     |

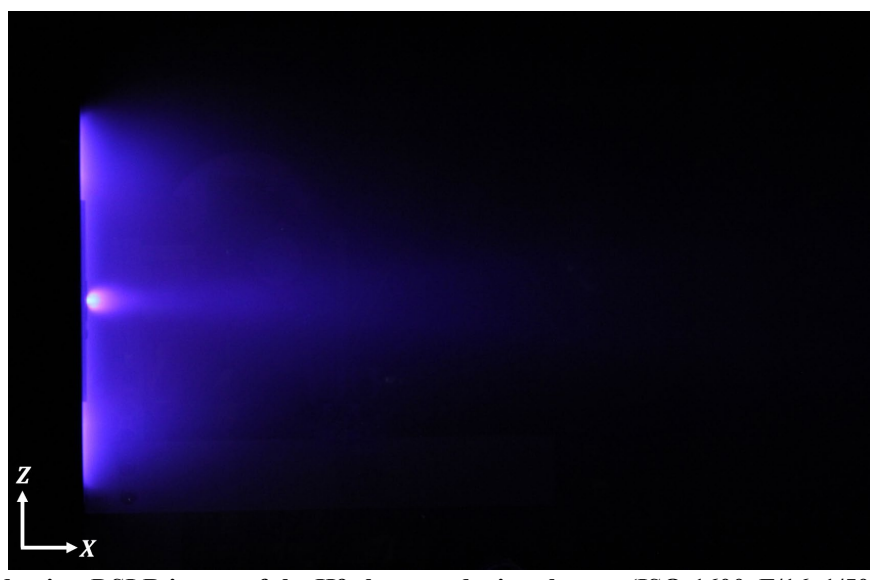


Figure 4. Side-view DSLR image of the H9 thruster during the test (ISO-1600, F/16, 1/500s exposure).

The results section first goes over the images altogether, and then picks two representative images to examine further. Vertical profiles were taken from these images at select distances downstream of the plume to plot brightness as a function of height, and to see how the cathode and anode discharge streams evolved as they moved down the plume. Next, relative beam intensity as a function of thruster radius was estimated using an inverse Abel transform on each image. Lastly, KrII and KrI images were combined for a heatmap of relative ion emission with respect to neutral emission.

#### A. Overall Images

Figure 5 shows the collection of images taken during thruster operation. These photographs are monochrome with artificially added color for ease of distinguishing between wavelengths. Some images contain Newton's rings, a photography artifact which causes circular ripples to emanate from the center of a picture<sup>29</sup>, visible in the 829.8 nm and 811.3 nm photographs. There are also background objects faintly present in some of the images, especially those in the top row of Fig. 5.



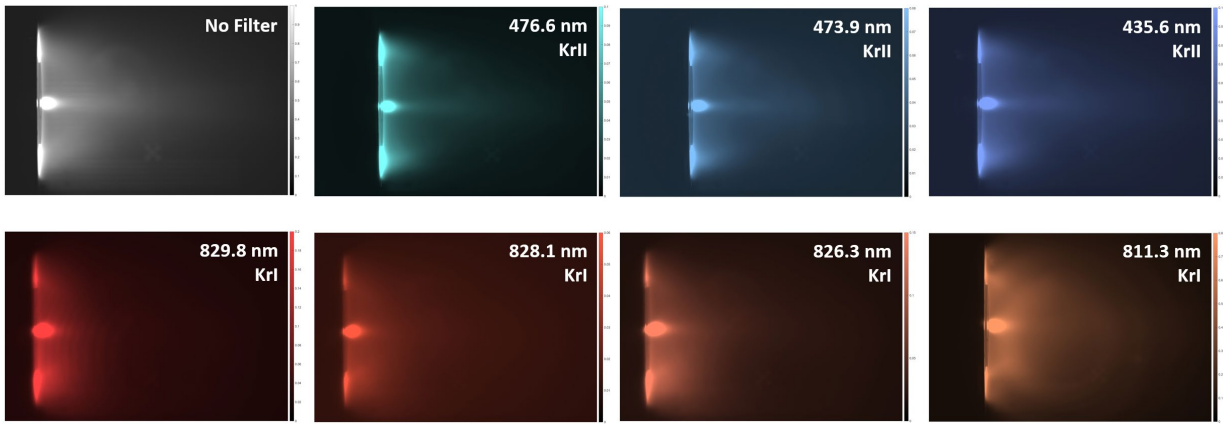


Figure 5. Monochrome images taken with each krypton filter. Wavelengths shown in the 400 nm range correspond to excited Kr ions (KrII) while wavelengths in the 800 nm range correspond to excited Kr neutrals (KrI). Images are artificially colored to help differentiate species categories.

In each image, there are bright plumes coming from both the cathode and the discharge channels. To remain consistent in nomenclature, we will refer to the anode as the discharge channel. In most images, the lower discharge channel is brighter than the upper channel. It is unclear whether this is due to a facility effect, background light, or the viewing angle of the camera aimed at the thruster.

Examining the neutral images in the bottom row, we can see a bright thin sliver of neutrals in the discharge channels right at the start of the thruster plume. This may be due to the camera looking back into the channels at a slight angle, allowing us to see neutral propellant that hasn't been accelerated out of the thruster. There is also high number of excited neutrals right in front of the thruster past the exit plane. This may be due to the acceleration region shifting further upstream than normal, due to the high background density in the chamber and channel, causing more of the electrons to be consumed by background neutrals.

#### **B.** Profile Analysis

Qualitatively comparing the plume shape between the Kr species in Fig. 5, the excited ion images converge inwards along the plume, while the excited neutral images diverge outwards from the thruster as a diffuse 'cloud', yet still and have some lines of convergence towards the middle of the thruster. To further investigate these images, in the following section we further investigate the 476.6 nm and 811.3 nm images as representatives of KrII and KrI, respectively. For visibility, the 476.6 nm and 811.3 nm images have been increased in both brightness and contrast.

Distances are described in units of 'thruster diameters' starting at the exit plane of the thruster. Intensity profiles for 8 columns of data very close to the exit plane (at distances of 15% thruster diameter and below) are illustrated below in Fig. 6, for both KrI and KrII. This short distance was selected in order to show profiles where the anode discharge plumes were most prominent.

The dashed lines represent the actual columns of data being analyzed, while the solid lines overlay the data sideways on top of the image. The raw data directly from the image contained some noise, so all brightness data was smoothed using a Gaussian-weighted moving average filter in MATLAB. For each profile, the data is normalized with respect to the integrated intensity under the curve. The local maxima of the bright anode discharge channels were used to trace the converging paths for the excited ions and neutrals., using a line of best-fit traced along the local maxima from the channel. Local maxima are marked in yellow dots, and the fitted line is traced in thin yellow dashes. The local maxima are plotted on the dashed lines and not the solid lines, since the solid curves are just projections of the brightness data along their respective dashed lines.



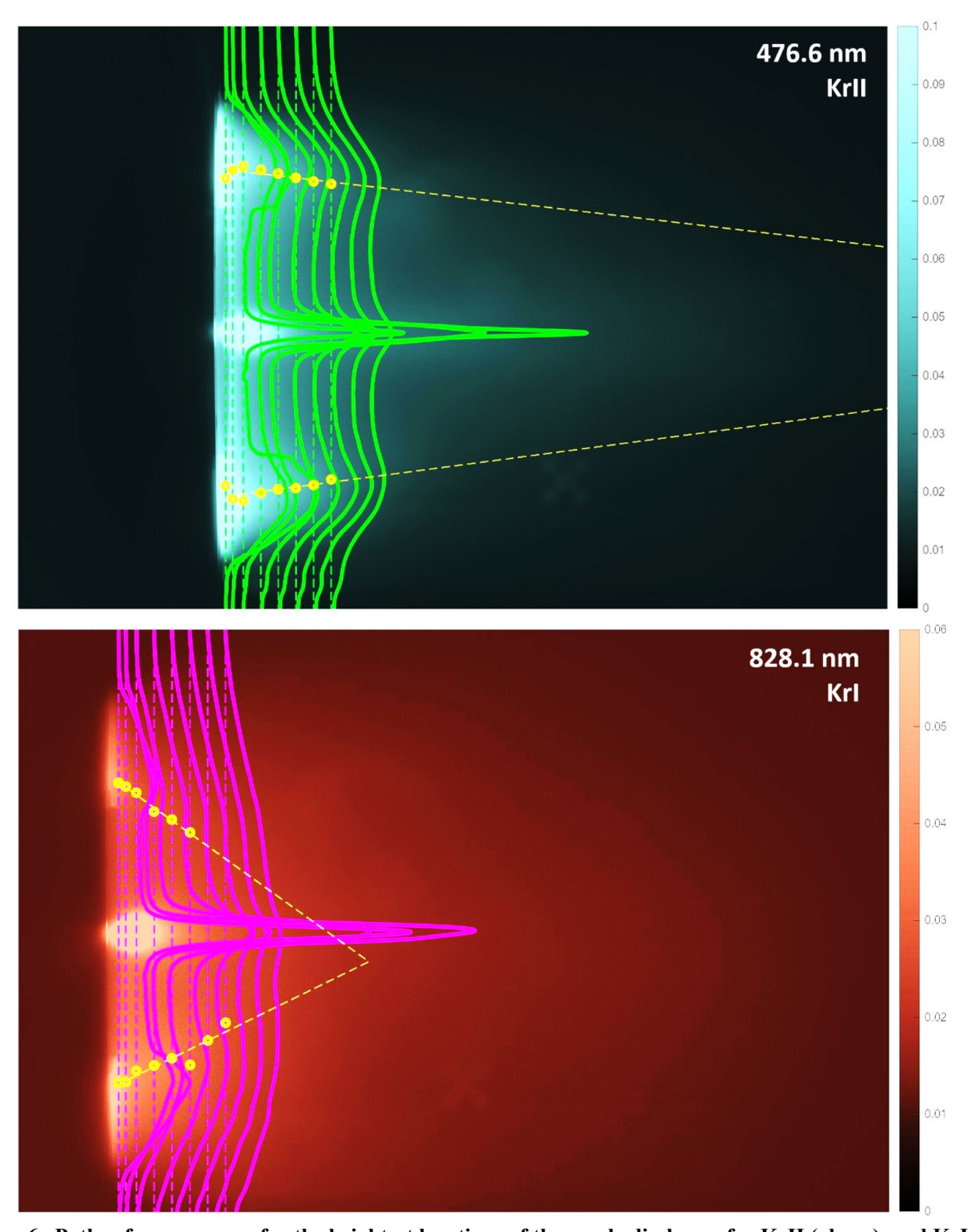


Figure 6. Paths of convergence for the brightest locations of the anode discharge for KrII (above), and KrI (below). For visibility, images are increased in both brightness and contrast.



It is observed in Fig. 6 that the brightest portions of the anode channel converge to the center of the plume sooner for neutral atoms than ions. Although the brightest neutrals converge inwards, there is still a 'cloud' of neutrals diverging outwards from the thruster exit plane visible in the image, which is not seen in the KrII image.

The KrII plot in Fig. 6 shows its brightest local maxima starting near the inside edge of the channel, then briefly bowing outward before converging inward again. The reason for this is unclear, but one possible explanation could be an imaging artifact due to the camera placement at a slight angle ahead of the thruster looking into the front of the channel. The KrI plot in Fig.6 shows an unusually asymmetric line of convergence, illustrated by the yellow dashed lines. This is likely an effect of the lower anode discharge channel being brighter than the upper anode discharge channel.

Figure 7 shows plots of image brightness at distances further down-plume. From left to right, the chosen lines are ahead of the exit plane at 1%, 20%, 40%, and 60% of one thruster diameter. In both images, the leftmost column of data, located 1% of a thruster diameter downstream, shows local maxima for the anode discharge channels, and a very prominent peak from the central cathode plume. Going further down the plume, the KrII plot maintains a local maximum for the anode discharge channel until the 40% line, while the KrI plot loses its prominent peaks by the 20% line.

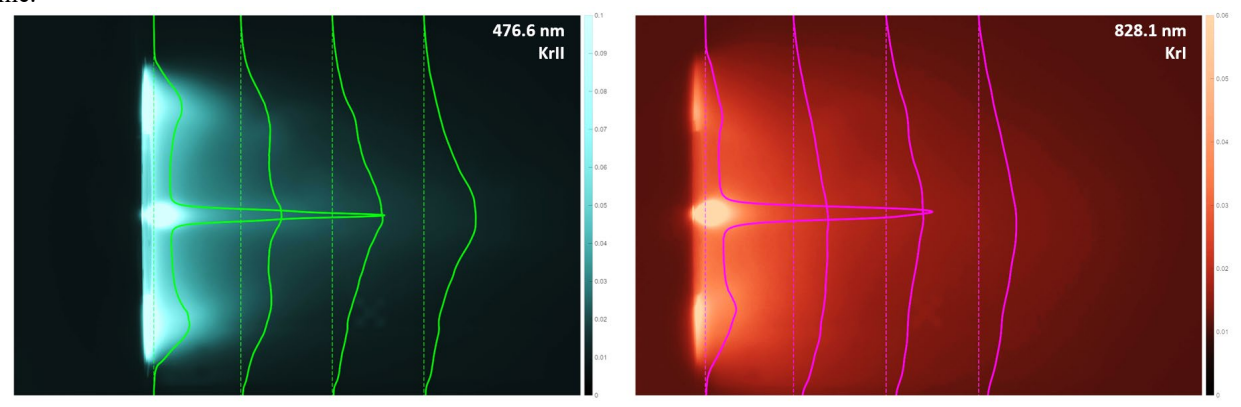


Figure 7. Profile analysis for both ions (left) and neutrals (right) at set distances downstream. For visibility, images are raised in both brightness and contrast.

#### C. Abel Inversion with Light Intensity Integration

With a vertical column of intensity data from a plume image, we are able to deconvolute an intensity profile into a radial profile of intensity using an inverse Abel transform. In this section, and as shown in Fig. 8, the vertical axis of this profile corresponds to a light intensity. Note that this intensity in not in units of photons or flux, but rather in arbitrary proportional units. In this sense, it can be thought of as a 'estimated local photon density'. This new radial profile can be described as a function of radius, i(r). This profile shows a significant peak in the cathode region, with almost negligible contribution from the anode region. To illustrate the contributions of both anode and cathode, we can find a radially normalized profile, I(r), by integrating i(r) by its annular area as r increases out from the center, using  $I(r) = 2\pi r i(r) dr$ . The process is illustrated below in Fig. 8.

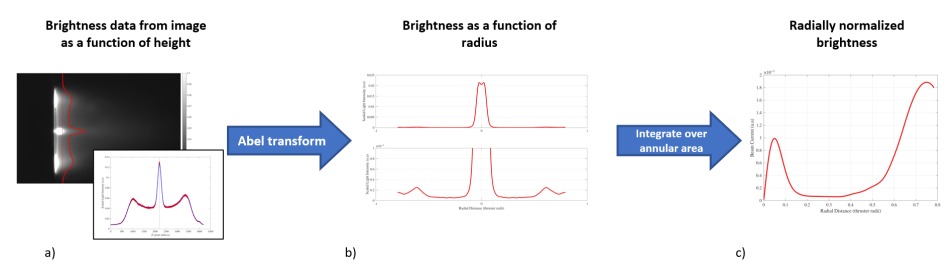


Figure 8. Process for obtaining a column of image data (a), and applying the Abel inversion (b) to retrieve a radially normalized brightness (c).



The left plot shows how a vertical slice of intensity data is taken from the original image. Between the left and center plots, an inverse Abel transform is applied to the brightness data to change the profile from a function of height into radius. The centermost plot is shown in 2 views to show that the intensity in the cathode plume is orders of magnitude greater than that of the anode discharge. After integrating over circular area to calculate a radially normalized intensity, the area for any ring in the anode region is significantly greater than the area in the cathode region, giving a high channel intensity, and a lowered cathode intensity, as shown in the rightmost plot of Fig. 8. Using this conversion, Figure 9 shows the radially normalized intensity plots as a function of radial distance, measured at a distance of 5% of the thruster diameter down the plume.

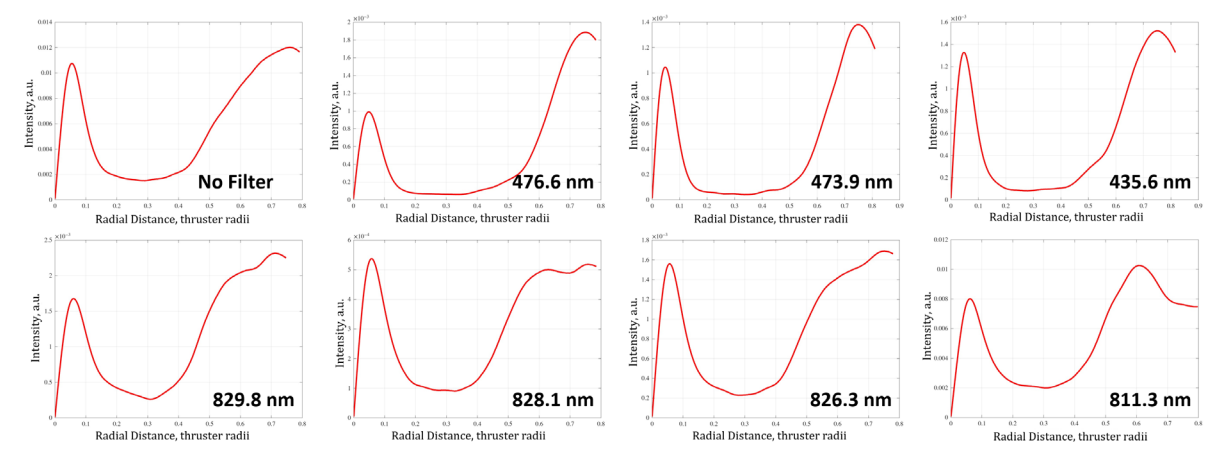


Figure 9. Radially normalized intensity vs radial distance, at 5% diameter length from the exit plane.

All the plots share similar behavior, with a high beam intensity in both the cathode and anode regions. The relationship between intensity magnitudes at the different wavelengths corresponds well with the relationship between magnitudes of brightness in the original images. This is because both the Abel inversion and the integral over the thruster area will scale linearly with brightness. The peaks present in the cathode region of each plot are expected, because this region has the combination of highest electron current, highest electron density, and highest neutral density in the plume. To examine the intensity profile further downstream, Fig. 10 shows the beam intensity as a function of radial distance, measured at a distance of 20% of the thruster diameter down the plume.

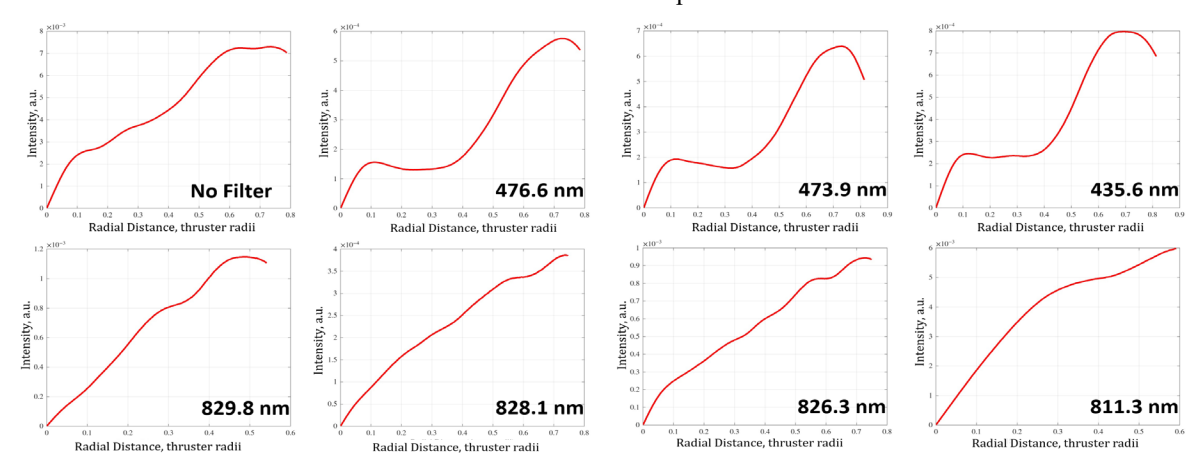


Figure 10. Intensity vs radial distance, at 20% diameter length from the exit plane.

In this plot, there is a distinct difference between the krypton neutral plots on the bottom row, and the three krypton ion plots in the top row. The krypton ions show a similar profile to the previous set in Fig. 9, but with reduced



magnitude and cathode intensity. The krypton neutrals show a steady increase outward from the thruster centerline without a distinct maximum for either the cathode or anode regions. In an ideal measurement, we would have a longer range of radius, extending further beyond the physical thruster to see the intensity drop off as the position exceeds the physical thruster radius.

We also investigate how the radial distance bounds seem to be truncated in the 20% length plots compared to the 5% length plots. This occurs when we have asymmetric plumes in our images, because for any given column of data, we truncate the height of the data set to be centered around the maximum brightest point. This issue becomes prominent in the neutral plots far downstream, where the intensities are most skewed in height. Recall Fig. 6, where the neutral plot showed a skewed path of convergence compared to the KrII ion plot.

## D. Image Stacking

With careful image alignment, and by scaling image brightness data to the OES data recorded during the test, we can stack pairs of images together to create heatmaps of the plume that tell where the ratios of ion to neutral spectral emission is highest and lowest. Figure 11 shows one such heatmap between 476.6 nm and 828.1 nm representing KrII singly charged ions and KrI neutral atoms respectively.

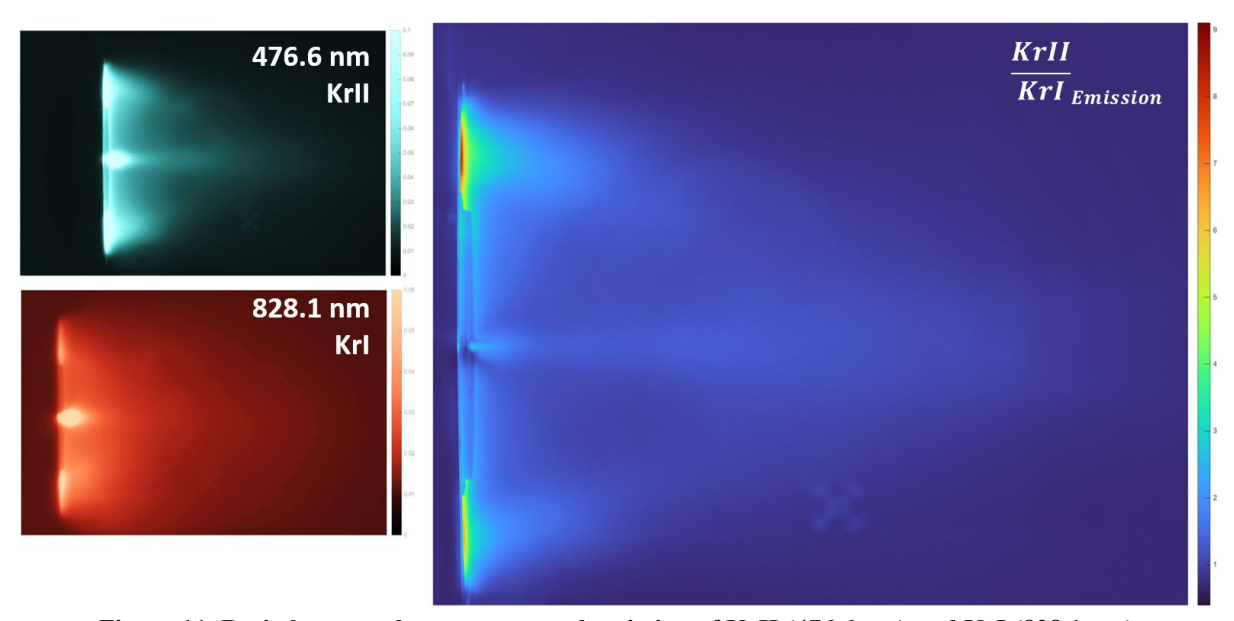


Figure 11. Ratio heatmap between spectral emission of KrII (476.6 nm) and KrI (828.1 nm).

Fig. 11 shows that the ions are converging down the plume. The near cathode region shows ions from the cathode plume; however, far downstream of the cathode we see the presence of excited ions and neutrals is likely due to the confluence of electrons borne at the cathode interacting with ion and neutral species from the cathode and the anode. To understand this complex spatial interplay of ions, electrons, and neutrals requires coupled experimental, theoretical, and computational analyses. For example, for future SpatialOES efforts we plan to use dissimilar gases (e.g., Xe and Kr) in the cathode and anode to gain further insight into the spatial behavior of the interactions between the electrons and anode and cathode borne species.

#### E. Other Details

Camera placement with respect to the thruster must be carefully aligned for accurate measurements. Ideally, the camera should be exactly in-line with the thruster exit plane. When the photographs were taken, the camera was about 3 cm in front of the exit plane. As a result, there is a small angle of view into the anode channel which may add uncertainties to the data closest to the front of the thruster about 0.7 degrees into the front of the thruster.

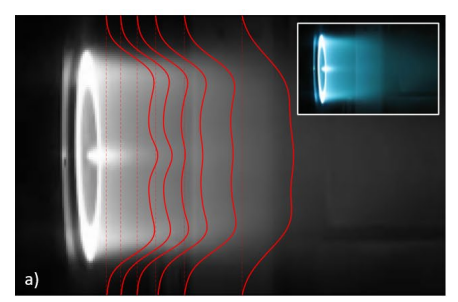
Another source of uncertainty is the altitude angle above horizontal that exists between the center of the camera lens and the very top or bottom edges of the thruster. The Abel transform assumes perfectly parallel views, but a real

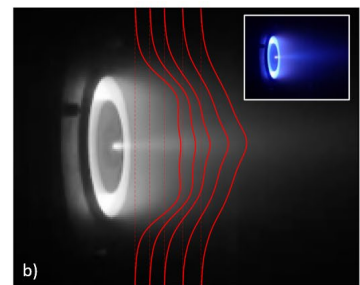


camera will have some range of field-of-view between the centermost pixel and outermost pixels. Given an estimated 15 cm thruster radius<sup>30</sup> and a distance of about 221 cm away from the camera, the widest angle from the camera lens to the top of the thruster is 3.9 degrees from horizontal. Future work is needed to determine whether this is an acceptable angle for our purposes, or if this angle should be decreased by increasing the distance from the thruster to the camera, or by using a longer focal length telephoto lens for a narrower field of view.

We have determined that the effect of gravity is not the cause of the difference in plume brightness between the upper and lower channels seen in Fig. 5. A quick calculation of thermal velocity will show that gravitational effects on the neutrals are insignificant compared to the high magnitude of krypton's thermal velocity, even at a minimum of 300 degrees Celsius.

The same image processing strategy of measuring intensity down a column of pixels can be applied to regular DSLR photos of thrusters as well, in order to qualitatively compare the overall plume. Spectroscopic information is lost since all visible light is being recorded by the camera, but these can be used to gain insight on how the thruster was affected by high background pressure. In Fig. 12, the first two plots show publicly available images of the H9 thruster plume taken with normal color DSLR cameras, compared to a color DSLR camera picture of the plume seen at the FIT-III test on the right. In the first two images, well defined local maxima from the anode discharge channels are present, extending far down-plume from the exit plane. In the third image, these peaks are less prominent and are not sustained nearly as far down the length of the plume. Despite being a very rough analysis, especially due to the high angle of view looking into the thruster faces and the low resolution of the images, these can still provide valuable information about the relationships between background pressure and thruster plumes.





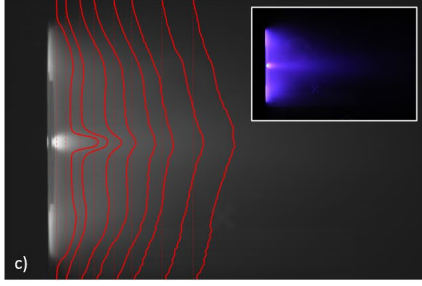


Figure 12. Brightness as a function of image height at set distances for a set of H9 photos available online (a), (b), compared to a color DSLR photo of the plume taken during the high-pressure test (c).

# V. Conclusion and Future Work

#### A. Conclusion

SpatialOES was used as a method of non-intrusively measuring the plume of a HET with a centrally mounted cathode. By using narrow bandpass filters centered at specific wavelengths, we distinguish between krypton neutral atoms, and singly charged krypton ions. Using the filtered images, we can visually identify points of interest in the plume and study the interactions between anode and cathode. By scaling data with respect to simultaneous OES measurements, we created 2D maps of relative photon intensity for specific wavelengths.

For images of neutrals and ions, we sliced images vertically at select distances down the plume to plot brightness with respect to image height. By applying an inverse Abel transform to the same slices of image data and integrating the results over the circular thruster area, estimations for a relative implied intensity can be retrieved as a function of radius. Heatmaps comparing the relative emission of ions and neutral wavelengths can be produced by carefully aligning the filtered images. This data will be valuable for use with collisional radiative models, which can be used to produce spatially resolved plots of electron temperature and density.

# **B.** Future Work

In this study, filtered images were taken for an internal-cathode-thruster, but future tests are planned to give a more comprehensive comparison between thruster configurations. The first priority is to test on another internal-cathode-



thruster using dissimilar propellants for the cathode and anode. During this test, we will use the camera and wavelength filters to look straight across the plume at different operating conditions. This will allow for a more complete and accurate comparison of cathode placement and species distribution. In order to minimize sources of noise and uncertainty, future tests should ensure that background objects are removed or hidden from view, and to keep the background as dark as reasonably possible. We hope to show that more thorough investigation with bandpass filters can provide additional insight into the characterization of plasma plumes for a variety of electric propulsion devices and operating conditions. In the long term, we plan to continue this study on more devices including radio-frequency gridded ion thrusters (GITs). We would also like to use SpatialOES to direct instruments with higher speed and less spatial capability such as *FastOES*, currently being developed by our research group<sup>31,32</sup>.

Improved smoothing techniques should be used with the radial reconstruction in later studies. The inverse Abel transform method used in this study was a simple tomographic operation to extract radial information from a side profile, but cascading inaccuracies can arise if the side data is not perfectly symmetric. Some basic smoothing was done within MATLAB to reduce the noise of the data, but future tests should employ more methods of preparing the data for the Abel transform and improved camera alignment. To process the data further, we plan to use the image data with collisional radiative models (CRMs) to spatially resolve electron temperature and density, including plans to collaborate with Colorado State University and NASA JPL on analysis of these results.

# VI. Acknowledgements

We would like to thank our funding from the Joint Advanced Propulsion Institute (NASA Grant No. 80NSSC21K1118) and Dr. Justin Koo's Propulsion and Power Program at the Air Force Office of Scientific Research (AFOSR Award No. FA9550-25-1-0012).

#### References

- <sup>1</sup>A Obenchain, R. A. and Wirz, R.E., (2025) Neutral Drift and Transport in Ion and Hall Thruster Test Facilities, IEPC, London, UK. (IEPC-2025-606)
- <sup>2</sup> Cretel, C. M. and Wirz, E. R., (2025). *Electric Propulsion Mission Life Prediction using a Multi-Fidelity Modeling Framework*, International Electric Propulsion Conference, London, UK. (IEPC-25-585)
- <sup>3</sup> Dragnea, H. C., Ortega, A. L., Kamhawi, H., & Boyd, I. D. (2020). Simulation of a Hall effect thruster using krypton propellant. *Journal of Propulsion and Power*, 36(3), 335-345.
- <sup>4</sup>Goebel, D. M., Jameson, K. K., & Hofer, R. R. (2012). Hall thruster cathode flow impact on coupling voltage and cathode life. *Journal of Propulsion and Power*, 28(2), 355-363.
  - <sup>5</sup> Potrivitu, George-Cristian. On the low-current hollow cathodes for electric propulsion for small satellites. Diss. 2022.
- <sup>6</sup> Tilley, D., de Grys, K., & Myers, R. (1999, June). Hall thruster-cathode coupling. In 35th Joint Propulsion Conference and Exhibit (p. 2865).
- <sup>7</sup> McDonald, M. S., & Gallimore, A. D. (2009, September). *Cathode position and orientation effects on cathode coupling in a 6-kW Hall thruster*, IEPC, Ann Arbor, Mi, USA. (IEPC-2009-113)
- <sup>8</sup> Hofer, R. R., Johnson, L. K., Goebel, D. M., & Wirz, R. E. (2008). Effects of internally mounted cathodes on Hall thruster plume properties. *IEEE Transactions on Plasma Science*, 36(5), 2004-2014.
- <sup>9</sup> Sommerville, J., & King, L. (2007). Effect of Cathode Position on Hall-Effect Thruster Performance and Near-Field Plume Properties. *In 44th AIAA/ASME/SAE/ASEE Joint Propulsion Conference & Exhibit* (p. 4996).
- <sup>10</sup> Xu, K. G., & Walker, M. L. (2014). Effect of external cathode azimuthal position on Hall-effect thruster plume and diagnostics. *Journal of Propulsion and Power*, 30(2), 506-513.
- <sup>11</sup> Byrne, M. P., Roberts, P. J., & Jorns, B. A. (2006). Coupling of electrical and pressure facility effects in hall effect thruster testing. *meta*, 5, 2.
- <sup>12</sup> Snyder, J. S., Lenguito, G., Frieman, J. D., Haag, T. W., & Mackey, J. A. (2020). Effects of background pressure on SPT-140 hall thruster performance. *Journal of Propulsion and Power*, *36*(5), 668-676.
- <sup>13</sup> Cusson, S. E., Jorns, B. A., & Gallimore, A. D. (2019, September). Impact of neutral density on the magnetic shielding of Hall thrusters. IEPC, Vienna, Austria. (IEPC-2019-276)
- <sup>14</sup> Chaplin, V. H., Johnson, L. K., Lobbia, R. B., Konopliv, M. F., Simka, T., & Wirz, R. E. (2022). Insights from collisional-radiative models of neutral and singly ionized xenon in Hall thrusters. *Journal of Propulsion and Power*, 38(5), 866-879.
- <sup>15</sup> Zatsarinny, O., & Bartschat, K. (2013). The B-spline R-matrix method for atomic processes: application to atomic structure, electron collisions and photoionization. *Journal of Physics B: Atomic, Molecular and Optical Physics*, 46(11), 112001.



- <sup>16</sup> Tisaev, M., Cretel, C. M., Biswas, S., and Wirz, R. E., (2025) *Plasma and Collisional Radiative Modeling for Xenon RF Thrusters*, IEPC, London, UK. (IEPC-2025-596)
- <sup>17</sup> Wirz. R.E., Obenchain. R. A., Cretel, C. M., Cowan. R. W., Franz. L. K., Hofbeck. I. J., Harteloo. A. M., Haist. B., Reed. A., Scatena. A. L., Madland. J., Biswas. S., Tisaev. M., Pendergrass. A., Breddan. M. D., Konopliv. M., Crandall. P., Sabiston. G., Rongione. N., Ottavio. A., Taghizadeh. E., Fernandez-Coppel. J., Marian. J., Parmer. S., Electric Propulsion Research Activities in the Plasma, Energy & Space Propulsion Laboratory. (IEPC-2025-661)
- <sup>18</sup> Konopliv, Mary, and Richard Wirz., (2024) *Cathode Species Contributions to Hall Thruster Plume* Dynamics, IEPC, Toulouse, France. (IEPC-2024-488)
- <sup>19</sup> Zhang, G., Ren, J., Liang, W., Ouyang, N., Lu, C., and Tang, H., "Coupling plasma plume of a low-power magnetically shielded Hall thruster with a hollow cathode," *Chinese Journal of Aeronautics*, Vol. 33, 2020
- <sup>20</sup> Lin, C. C. (2011, April 7). Krypton Energy Level Diagram. University of Wisconsin Atomic Collisions Group. http://raptor.physics.wisc.edu/data/data.htm?
- <sup>21</sup> Gangwar, R. K., Srivastava, R., & Stafford, L. (2016). Spectroscopic diagnostics of low-pressure inductively coupled Kr plasma using a collisional–radiative model with fully relativistic cross sections. *Plasma Sources Science and Technology*, 25(3), 035025.
- <sup>22</sup> Wirz, R. E. (2025). Spatiotemporal characterization of canonical RF discharges with and without ion extraction. 2025 Propulsion and Power Annual Review, AFOSR.
- <sup>23</sup> Kramida, A., Ralchenko, Yu., Reader, J., and NIST ASD Team (2024). *NIST Atomic Spectra Database* (ver. 5.12), [Online]. Available: https://physics.nist.gov/asd [2025, September 2]. National Institute of Standards and Technology, Gaithersburg, MD. DOI: https://doi.org/10.18434/T4W30F
- <sup>24</sup> Lee, D., Kim, J., Doh, G., Shin, C., & Choe, W. (2022). Two-dimensional electron temperature and density profiles of Hall thruster plume plasmas using tomographically reconstructed optical emission spectroscopy. *Plasma Sources Science and Technology*, 31(12), 125004.
  - <sup>25</sup> Urban, P. J. (2018). Non-Intrusive Optical Measurement of Electron Temperature in Near Field Plume of Hall Thruster.
- <sup>26</sup> Jameson, K., Goebel, D., & Watkins, R. (2007, July). Neutral Density Measurements in a Hall Thruster Plume. In 43rd AIAA/ASME/SAE/ASEE Joint Propulsion Conference & Exhibit (p. 5853).
  - <sup>27</sup> Feeman, T. G. (2010). *The mathematics of medical imaging*. Springer New York.
- <sup>28</sup> Hofer, R. R., Cusson, S. E., Lobbia, R. B., & Gallimore, A. D. (2017, October). The H9 magnetically shielded Hall thruster. IEPC, Atlanta, GA, USA (IEPC-2017-232).
  - <sup>29</sup> Goodwin, E. P., & Wyant, J. C. (2006). Field guide to interferometric optical testing. Bellingham, WA: SPIE.
- <sup>30</sup> Brown, Z. A., & Jorns, B. A. (2023). Growth and saturation of the electron drift instability in a crossed field plasma. *Physical Review Letters*, 130(11), 115101.
- <sup>31</sup> Harteloo, A. M. and Wirz, R. E., (2025) *Broadband Characterization of Hall Thruster Discharge and Cathode Multimode Plasma Oscillations via FastOES*, IEPC, London, UK. (IEPC-2025-665)
- <sup>32</sup> Konopliv, Mary, Timothy Simka, Richard Wirz, Robert Lobbia, and Lee Johnson. (2022). Fast Optical Emission Spectroscopy for Studying Plasma Behavior in Hall Thrusters, IEPC, Cambridge, MA, USA. (IEPC-2022-171)

